J Mol Model (2006) 12: 569–576
DOI 10.1007/s00894-005-0035-5

ORIGINAL PAPER

Anastassia N. Alexandrova · Eldon Koyle
Alexander I. Boldyrev

Theoretical study of hydrogenation of the doubly aromatic B_7^- cluster

Received: 8 March 2005 / Accepted: 29 July 2005 / Published online: 29 October 2005

Abstract We have studied the influence of hydrogenation on the relative stability of the low-lying isomers of the anionic B_7^- cluster, computationally. It is known that the pure-boron B_7^- cluster has a doubly (σ- and π-) aromatic C_{6v} ($^3A_1$) quasi-planar wheel-type triplet global minimum (structure 1), a low-lying σ-aromatic and π-antiaromatic quasi-planar singlet C_{2v} ($^1A_1$) isomer **2** (0.7 kcal mol^{-1} above the global minimum), and a planar doubly (σ- and π-) antiaromatic C_{2v} ($^1A_1$) isomer **3** (7.8 kcal mol^{-1} above the global minimum). However, upon hydrogenation, an inversion in the stability of the species occurs. The planar $B_7H_2^-$ (C_{2v}, $^1A_1$) isomer **4**, originated from the addition of two hydrogen atoms to the doubly antiaromatic B_7^- isomer **3**, becomes the global minimum structure. The second most stable $B_7H_2^-$ isomer **5**, originated from the quasi-planar triplet wheel isomer **1** of B_7^-, was found to be 27 kcal mol^{-1} higher in energy. The inversion in stability occurs due to the loss of the doubly aromatic character in the wheel-type global minimum isomer (C_{6v}, $^3A_1$) of B_7^- upon H_2–addition. In contrast, the planar isomer of B_7^- (C_{2v}, $^1A_1$) gains aromatic character upon addition of two hydrogen atoms, which makes it more stable.

Keywords Multiple aromaticity · Boron hydrides · Boron clusters

Dedicated to Professor Dr. Paul von Ragué Schleyer on the occasion of his 75th birthday.

A. N. Alexandrova · E. Koyle · A. I. Boldyrev (✉)
Department of Chemistry and Biochemistry,
Utah State University, 0300 Old Main Hill,
Logan, UT 84322-0300, USA
E-mail: Boldyrev@cc.usu.edu
Tel.: +1-435-7971630
Fax: +1-435-7973390

Introduction

Pure-boron clusters have received much attention in the literature over the past couple of decades [1–12]. The geometries and electronic properties of these species were addressed, while sometimes the results obtained by different groups were not in agreement. Recently, we published a series of articles on the chemical bonding of neutral and anionic planar or quasi-planar pure-boron clusters from B_3 to B_{15} [13–18]. Both theoretical and photoelectron spectroscopic characterizations were performed for these species. We have explained the planar or quasi-planar structure of small boron clusters on the basis of the presence of double (σ- and π-) aromaticity, or σ- and π-antiaromaticity, or a mixture of them. Double aromaticity (the simultaneous presence of σ- and π-aromaticity) was introduced in chemistry by Schleyer and coworkers [19] in the late 1970 s for explaining properties of the 3,5-dehydrophenyl cation. Double aromaticity and antiaromaticity were first used by Martin-Santamaria and Rzepa [20] for explaining chemical bonding in small carbon rings. Berndt and coworkers have shown that small carborane molecules containing three- and four-membered rings also exhibit both σ- and π-aromaticity [21–25]. Double aromaticity in boron clusters forces them to adopt the wheel-type structures, such as D_{7h} ($^1A_1'$) B_8^{2-} or D_{8h} ($^1A_{1\,g}$) B_9^- [17], while the doubly antiaromatic boron clusters, such as B_6^{2-} [15], adopt highly distorted polygonal topology. Switching from an aromatic form to an antiaromatic form and vice versa can be accomplished by adding or removing a pair of electrons, or by forming two B-H bonds during the partial hydrogenation of boron clusters.

We thought that it would be important to understand how hydrogenation may affect the structure of boron clusters, because when 1:1 hydrogenation is reached, a transformation from planar or quasi-planar structures of pure-boron clusters into 3D structures of hydrogenated species is expected. The $B_xH_x^{2-}$ boranes are known to have deltahedral structures [26–28].

Hydrogenated small boron clusters have been studied before. Ricca and Bauschlicher characterized cationic B_nH^+ clusters theoretically [29]. Small systems B_2H^+, $B_2H_2^+$, and $B_3H_2^+$ were studied by Curtiss and Pople [30]. Larger B_nH_n species ($n = 3-6$) were calculated by many groups using ab initio methods (see reference [31] and references therein). A series of theoretical and experimental studies on other similar systems have been reported by various authors [32–34]. Experimental and theoretical studies of the pure B_7 cluster in neutral and various ionic forms were also previously reported [8, 35–39]. The B_7^- anion has a triplet doubly (σ- and π-) aromatic C_{6v} ($^3A_1$) quasi-planar wheel-type global minimum, a low-lying singlet σ-aromatic and π-antiaromatic C_{2v} ($^1A_1$) quasi-planar isomer (0.7 kcal mol^{-1} above the global minimum), and a planar doubly (σ- and π-) antiaromatic C_{2v} ($^1A_1$) isomer [16].

In the current article we present results of our theoretical study of the hydrogenation of a doubly aromatic boron cluster B_7^-. This includes our computational results on the relative stability of low-lying B_7^- isomers upon the influence of addition of two hydrogen atoms.

Computational methods

While the structure of the B_7^- anion was firmly established in our previous work [16], we decided to perform the search for its global minimum again in order to test our Gradient Embedded Genetic Algorithm (GEGA) program, written by Alexandrova et al. [40]. We then used the GEGA program to find low-lying isomers for the $B_7H_2^-$ anion also. The GEGA procedure [40] is based upon the geometry interplay proposed by Hartke [41] and Deaven and Ho [42], and involves some unique mutation and optimization specifics. The hybrid method, known as B3LYP [43–45], with relatively small basis set 3-21G was employed throughout the execution of the GEGA. Briefly, within the GEGA procedure, the initial geometries of individuals in the population are randomly generated and further optimized to the nearest local minima on the potential energy surface, using the Gaussian 03 package [46]. If a saddle point is encountered, the normal mode of the first imaginary frequency is followed until a local minimum is found. Then the population, composed of the good individuals thus selected, undergoes breeding and mutations. Probabilities to be bred are assigned according to the best-fit (lowest-energy) criterion. Based on these probabilities, pairs of parents are selected randomly. The geometries of the parents are cut by a random cutting plane, and the halves thus obtained (genes) are then recombined either in a simple or in a head-to-tail manner forming a child. The number of atoms in the newly generated geometry is checked, and the child is optimized to the nearest local minimum. After the number of individuals in the population has doubled within the breeding process, the best-fit group is selected and convergence of the algorithm is checked. The GEGA is considered converged if the current lowest energy species (global minimum or at least very stable local minimum) remains leading for 20 iterations. If convergence is not yet met, the highest energy species in the population undergo mutations. The mutation rate is set to 33.33%. Mutations are shifts of random atoms of a species in random directions, with the purpose of changing the initial geometry so as to push the structure out of the current local minimum to another well on the potential energy surface. Mutants are optimized to the nearest local minima. After that, the algorithm proceeds with the new cycle of breeding. All low-lying isomers are detected and stored throughout the execution and they are reported to the user at the end of the run. A few runs of GEGA are done on the system in order to confirm the global minimum structure found.

The geometry and vibrational frequencies of the global minimum thus identified, as well as low-lying isomers, were refined further at higher levels of theory. The B3LYP and coupled-cluster CCSD(T) [47–49] methods with polarized split-valence basis sets (6-311++G**) [50, 51] were used for this purpose. We also optimized geometry and calculated frequencies for the $B_7H_2^-$ global minimum structure at the CASSCF(4,4)/6-311++G** [52–57] level of theory. Single-point calculations were performed at the CASSCF(8,8)/6-311++G**//CASSCF(4,4)/6-311++G** level of theory in order to test the applicability of the B3LYP and CCSD(T) methods. The Natural Bond Order (NBO) analysis [58–62] was used for detailed chemical bonding examination. Molecular orbitals (MOs) were calculated at the HF/6-311++G** level of theory. B3LYP, HF, and CCSD(T) calculations were performed using the Gaussian 03 program. MOs were made using the MOLDEN 3.4 program [63].

Computational results and discussion

The GEGA search revealed the same three low-lying isomers **1**–**3** (Fig. 1) for B_7^- as we reported in our previous work [16]. Thus, our GEGA program performed well. The search for the most stable structure of the $B_7H_2^-$ anion, performed by GEGA and accompanied by the higher level calculations, revealed that the planar **4** (C_{2v}, $^1A_1$) (Fig. 2) structure is the global minimum. The order of the lowest structures for $B_7H_2^-$ was the same at the B3LYP/3-21G, B3LYP/6-311+G*, and CCSD(T)/6-311+G* levels of theory. The global minimum $B_7H_2^-$ cluster has the following electronic configuration: $1a_1^2 1b_2^2 2a_1^2 2b_2^2 3a_1^2 4a_1^2 3b_2^2 1b_1^2 4b_2^2 5a_1^2 6a_1^2 1a_2^2$. The molecular properties of the global minimum structure at three levels of theory are summarized in Table 1. The geometric parameters and harmonic frequencies calculated at these levels of theory were in reasonable agreement with each other. The Hartree–Fock configuration was found to be dominant ($C_{HF} = 0.969$) in the CASSCF(8,8)/

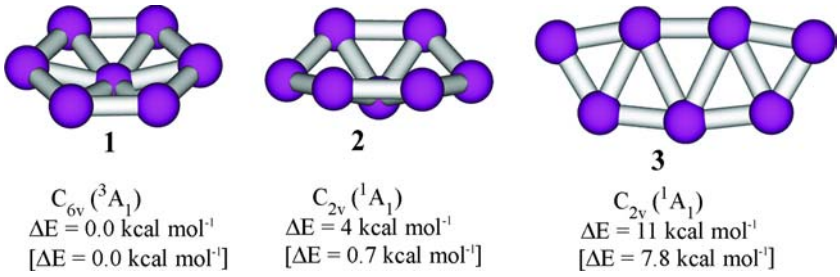

Fig. 1 Low-energy isomers of the B_7^- cluster at the B3LYP/6-311 + G* level of theory (relative energies computed at the CCSD(T)/6-311 + G(2df) level are shown in square brackets)

6-311 ++ G** expansion and thus our B3LYP and CCSD(T) calculations should be reliable.

The second lowest isomer (structure 5 in Fig. 2) is 27 kcal mol^{-1} higher in energy at the B3LYP/6-311 ++ G** level of theory. Molecular properties of the second isomer at B3LYP/6-311 ++ G** and CCSD(T)/6-311 ++ G** levels of theory are summarized in Table 2. All low-energy structures of $B_7H_2^-$ identified are shown in Fig. 2. The global minimum of $B_7H_2^-$ is a planar species; it originates from the planar isomer **3** of the bare B_7^- cluster (Fig. 1) with two hydrogen atoms bonded to the end boron atoms of the cluster. Other alternative isomers **8**, **10**, and **14**, having hydrogen atoms bound in different positions, also derive from the structure 3 of B_7^-. Among the isomers depicted in Fig. 2, the singlet and triplet species **5**–**7**, **9**, **11**, **12**, and **15** arise from either the isomer **1** or isomer **2** of B_7^- with different bonding positions of hydrogen atoms.

Thus, the addition of two hydrogen atoms completely rearranges the relative stability of the isomers of B_7^-. In the following section, we present our explanation of why that is happening.

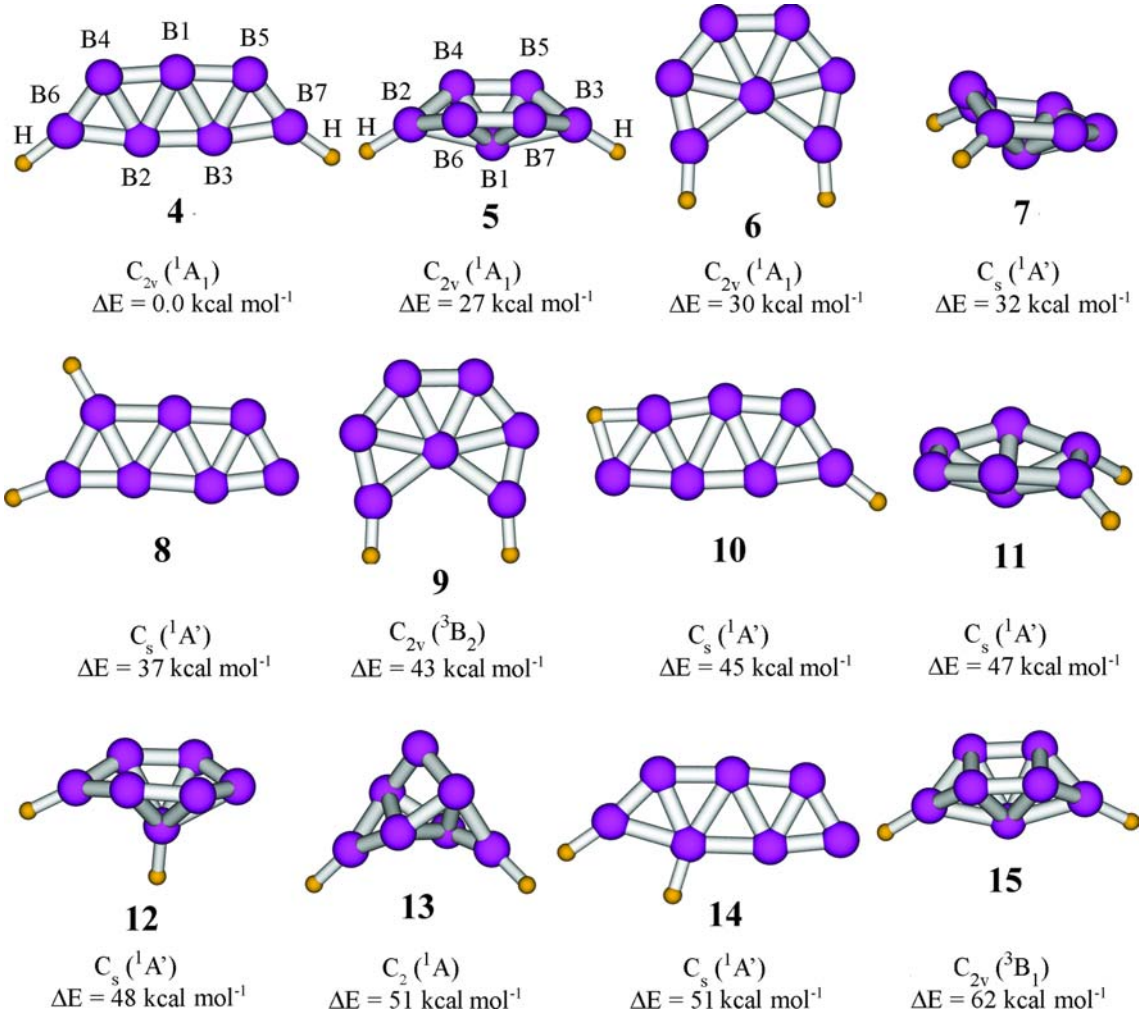

Fig. 2 Alternative structures of the $B_7H_2^-$ hydride (B3LYP/6-311 ++ G** level of theory)

Table 1 Molecular properties of the $B_7H_2^-$ (C_{2v}, $^1A_1$) global minimum species

	B3LYP/6-311++G**		CASSCF(4,4)/6-311++G**		CCSD(T)/6-311++G**
E_{total}, a.u.	−175.143862		−173.860826[b]		−174.554521
ZPE, kcal mol^{-1}	27.452		29.468		[c]
Geometry	R(B1-B2,3) = 1.7496 Å R(B1-B4,5) = 1.5954 Å R(B4-B6,7) = 1.5166 Å R(B2-B3) = 1.5975 Å R(B2-B6) = 1.6730 Å R(B6-H) = 1.1833 Å R(B4-B2) = 1.6763 Å ∠(B4-B6-H) = 162.895°		R(B1-B2) = 1.7859 Å R(B1-B4) = 1.5969 Å R(B4-B6) = 1.5087 Å R(B2-B3) = 1.6150 Å R(B2-B6) = 1.6938 Å R(B6-H) = 1.1815 Å R(B4-B2) = 1.6910 Å ∠(B4-B6-H) = 163.756°		R(B1-B2) = 1.7735 Å R(B1-B4) = 1.6179 Å R(B4-B6) = 1.5428 Å R(B2-B3) = 1.6196 Å R(B2-B6) = 1.6884 Å R(B6-H) = 1.1902 Å R(B4-B2) = 1.7071 Å ∠(B4-B6-H) = 162.245°
Frequencies, cm^{-1}	$\omega_1(a_1)$ 2686 (84)[a] $\omega_2(a_1)$ 1312 (8) $\omega_3(a_1)$ 1210 (0) $\omega_4(a_1)$ 858 (8) $\omega_5(a_1)$ 754 (13) $\omega_6(a_1)$ 683 (1) $\omega_7(a_1)$ 566 (12) $\omega_8(a_1)$ 381 (0) $\omega_9(a_2)$ 731 (0) $\omega_{10}(a_2)$ 471 (0) $\omega_{11}(a_2)$ 258 (0)	$\omega_{12}(b_1)$ 705 (1) $\omega_{13}(b_1)$ 469 (2) $\omega_{14}(b_1)$ 168 (1) $\omega_{15}(b_2)$ 2684 (284) $\omega_{16}(b_2)$ 1314 (14) $\omega_{17}(b_2)$ 1128 (2) $\omega_{18}(b_2)$ 897 (10) $\omega_{19}(b_2)$ 767 (0) $\omega_{20}(b_2)$ 641 (17) $\omega_{21}(b_2)$ 521 (0)	$\omega_1(a_1)$ 2766 $\omega_2(a_1)$ 2042 $\omega_3(a_1)$ 932 $\omega_4(a_1)$ 794 $\omega_5(a_1)$ 726 $\omega_6(a_1)$ 642 $\omega_7(a_1)$ 567 $\omega_8(a_1)$ 398 $\omega_9(a_2)$ 809 $\omega_{10}(a_2)$ 480 $\omega_{11}(a_2)$ 174	$\omega_{12}(b_1)$ 764 $\omega_{13}(b_1)$ 485 $\omega_{14}(b_1)$ 166 $\omega_{15}(b_2)$ 2762 $\omega_{16}(b_2)$ 1381 $\omega_{17}(b_2)$ 1362 $\omega_{18}(b_2)$ 1151 $\omega_{19}(b_2)$ 882 $\omega_{20}(b_2)$ 809 $\omega_{21}(b_2)$ 523	[c]

[a]Infrared intensities (km mol^{-1}) are shown in parentheses
[b]At the CASSCF(8,8)/6-311++G**//CASSCF/6-311++G** level $E_{total} = -173.891026$ a. u., $C_{HF} = 0.969$
[c]Vibrational frequencies were not calculated at this level of theory

Chemical bonding in $B_7H_2^-$ isomers

First, we performed an NBO analysis of the global minimum structure of $B_7H_2^-$. We found nine classical 2c–2e bonds, seven of which are localized on the peripheral edges of the B_7^- unit (bonds B1–B4, B4–B6, B6–B2, B2–B3, B3–B7, B7–B5, B5–B1, see Fig. 2), and the remaining two are simply covalent B–H bonds. The rest of the electrons in the system participate in delocalized bonding over the entire cluster. A similar bonding picture was found in structure 3 of the bare B_7^- species. The NBO analysis showed the presence of seven peripheral 2c–2e B–B bonds in the B_7^- cluster. However, the difference between the dihydride and the original B_7^- cluster occurs in the structure of delocalized bonding patterns.

The MOs of the global minimum isomer of $B_7H_2^-$ are shown in Fig. 3a. Figure 3b represents the MOs of the structure 3 of the bare B_7^- cluster. In order to elucidate the MOs responsible for the localized bonding, described

Table 2 Molecular properties of the second isomer of $B_7H_2^-$ (C_{2v}, $^1A_1$) – species **2**, Figure 1

	B3LYP/6-311++G**		CCSD(T)/6-311++G**
E_{total}, a.u.	−175.100763		−174.53084463
ZPE, kcal mol^{-1}	27.592		[b]
Geometry	R(B1-B2,3) = 1.9267 Å R(B1-B4,5,6,7) = 1.6640 Å R(B4-B5) = 1.5905 Å R(B2-B3) = 3.7470 Å R(B2-B4) = 1.6232 Å R(B2-H) = 1.1956 Å ∠(B1-B2-H) = 133.181°		R(B1-B2,3) = 1.9338 Å R(B1-B4,5,6,7) = 1.6901 Å R(B4-B5) = 1.6175 Å R(B2-B3) = 3.7730 Å R(B2-B4) = 1.6462 Å R(B2-H) = 1.1981 Å ∠(B1-B2-H) = 133.283°
Frequencies, cm^{-1}	$\omega_1(a_1)$ 2572 (83)[a] $\omega_2(a_1)$ 1277 (1) $\omega_3(a_1)$ 967 (6) $\omega_4(a_1)$ 757 (7) $\omega_5(a_1)$ 695 (0) $\omega_6(a_1)$ 438 (0) $\omega_7(a_1)$ 272 (0) $\omega_8(a_2)$ 875 (0) $\omega_9(a_2)$ 818 (0) $\omega_{10}(a_2)$ 614 (0) $\omega_{11}(a_2)$ 359 (0)	$\omega_{12}(b_1)$ 1109 (9) $\omega_{13}(b_1)$ 823 (11) $\omega_{14}(b_1)$ 566 (16) $\omega_{15}(b_2)$ 2570 (409) $\omega_{16}(b_2)$ 1032 (1) $\omega_{17}(b_2)$ 1015 (25) $\omega_{18}(b_2)$ 901 (31) $\omega_{19}(b_2)$ 792 (12) $\omega_{20}(b_2)$ 484 (1) $\omega_{21}(b_2)$ 317 (62)	[b]

[a]Infrared intensities are shown in parentheses
[b]Vibrational frequencies were not calculated at this level of theory

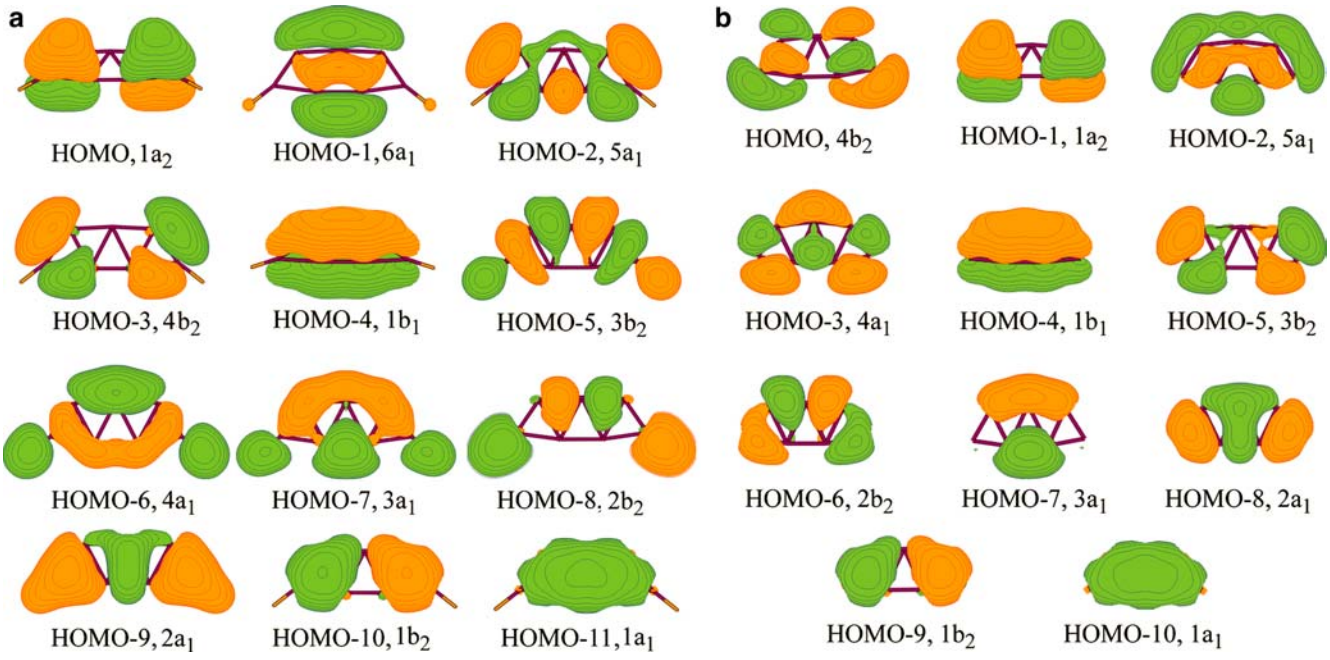

Fig. 3 Molecular orbital picture of **a** the global minimum of $B_7H_2^-$ (C_{2v}, $^1A_1$) and **b** of the bare B_7^- cluster (C_{2v}, $^1A_1$)

above, we performed an NBO calculation on the $B_7H_2^{5+}$ cation. We found that if the HOMO-2, HOMO-3, HOMO-5, HOMO-6, HOMO-7, HOMO-8, HOMO-9, HOMO-10, and HOM0-11 are occupied in $B_7H_2^{5+}$, the MOs can be localized into seven 2c–2e bonds as explained earlier. Thus, the localized bonding described is due to the presence of these low-lying MOs. The remaining HOMO, HOMO-1, and HOMO-4 are responsible for the bonding over the whole system. A similar analysis performed on the bare B_7^- cluster revealed that HOMO-3, HOMO-5, HOMO-6, HOMO-7, HOMO-8, HOMO-9, and HOMO-10 (Fig. 3b) form the peripheral σ-framework, while the remaining MOs represent delocalized bonding in the cluster. One may notice that, upon the introduction of two electrons to the system (addition of two H-atoms), the localized bonding region is enriched with two classical 2c–2e B–H bonds. Correspondingly, the delocalized region sacrifices one molecular orbital. Indeed, the HOMO of the B_7^- cluster is missing in $B_7H_2^-$, while the HOMO-1 in B_7^- corresponds to the HOMO in $B_7H_2^-$, the HOMO-2 corresponds to the HOMO-1 in $B_7H_2^-$, and the shapes of the HOMO-4 are identical in the two species (see Fig. 3).

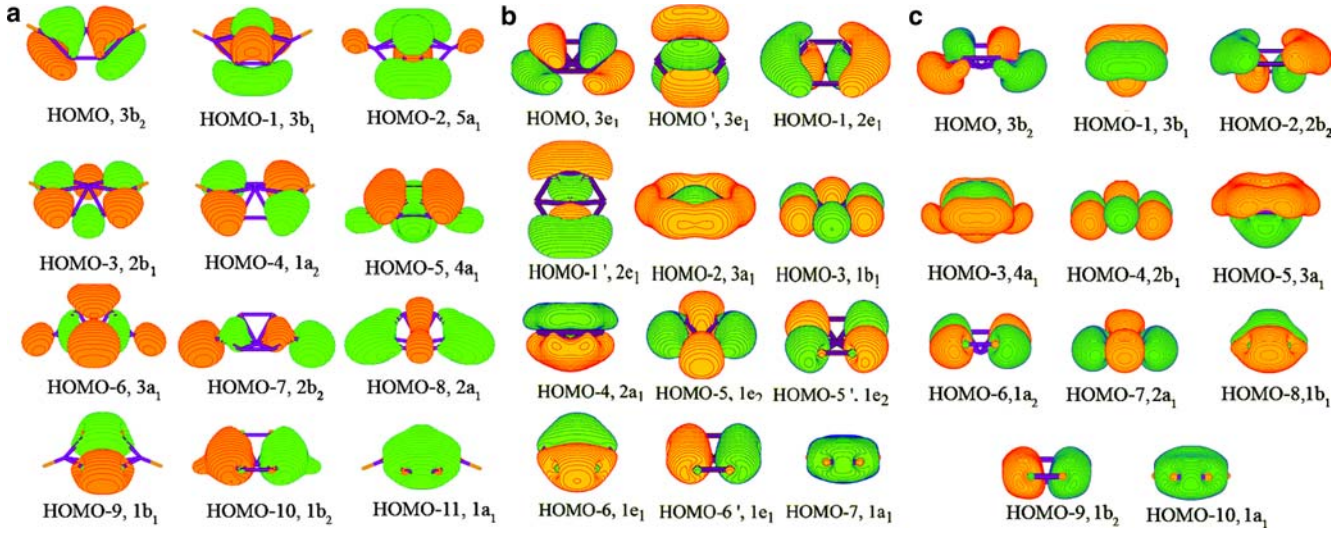

Fig. 4 Molecular orbital picture of **a** the second isomer of $B_7H_2^-$ (C_{2v}, $^1A_1$), **b** of the bare global minimum B_7^- cluster (C_{6v}, $^3A_1$), and **c** of the C_{2v}, $^1A_1$ isomer 2 of B_7^-

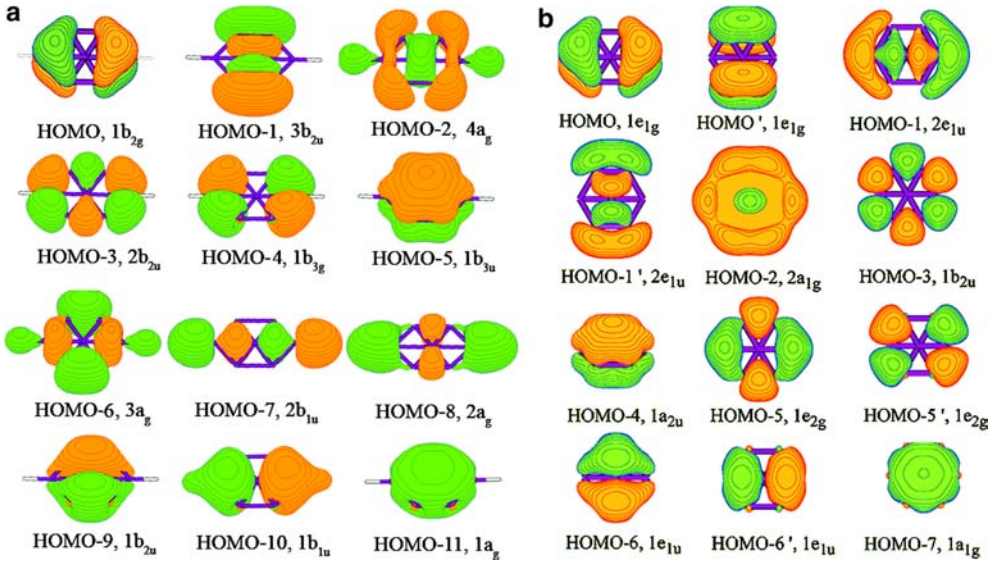

Fig. 5 Adjusted to the planarity molecular orbital picture of **a** the second isomer of $B_7H_2^-$ and **b** of the bare B_7^- cluster with corresponding geometry

As has been discussed in our previous work [16], the planar isomer **3** of the B_7^- cluster possesses doubly antiaromatic character. The HOMO-4 ($1b_1$) is a completely bonding π-molecular orbital, and the HOMO-1 ($1a_2$) is partially bonding π-MO with one nodal plane. Four π-electrons on these MOs make structure 3 of B_7^- π-antiaromatic. The HOMO-2 ($5a_1$) and the HOMO ($4b_2$) are MOs of σ-type formed by the radial overlap of the 2p-AOs on boron atoms, where the former MO is completely bonding, and the latter one is partially bonding. Hence, the four electrons occupying these MOs make the system also σ-antiaromatic.

In the hydride, the partially bonding σ-molecular orbital (HOMO in B_7^-) mentioned earlier is now a virtual orbital. The only delocalized σ-MO in the species is the HOMO-1 ($6a_1$) (Fig. 3a). Since the cluster obeys the $(4n+2)$ Hückel rule for aromatic compounds, it possesses σ-aromaticity. The π-MOs in the $B_7H_2^-$ cluster are analogous to those in the B_7^- species. Four electrons in these MOs make the global minimum of $B_7H_2^-$ π-antiaromatic. Consequently, upon the molecular hydrogen addition, the planar B_7^- cluster gains σ-aromaticity and loses the antibonding character in the σ-set of MOs.

We also performed a molecular orbital analysis for the wheel-type B_7^- and $B_7H_2^-$ moieties. The MOs of these species are shown in Fig. 4. Figure 5 depicts the MOs of the clusters in a simplified manner, that is, when geometries of both clusters are adjusted to planarity. This adjustment is done in order to make the bonding picture clearer (the sets of valence MOs shown are analogous to the ones in the original species). Removal of the electrons from the HOMO, HOMO-1, HOMO-2, and HOMO-5 (Fig. 5a) in $B_7H_2^-$ and subsequent localization demonstrates that the remaining MOs are responsible for the formation of six 2c–2e B–B bonds: B2–B4, B4–B5, B5–B3, B3–B7, B7–B6, B6–B2, and two B–H bonds. Similarly, in the B_7^- (C_{6v}, $^3A_1$) cluster, removal of electrons from the HOMO, HOMO′, HOMO-1, HOMO-1′, HOMO-2, and HOMO-4 (Fig. 5b) leaves the cluster with six peripheral B–B σ-bonds forming the six-membered ring. Thus, HOMO, HOMO-1, HOMO-2, and

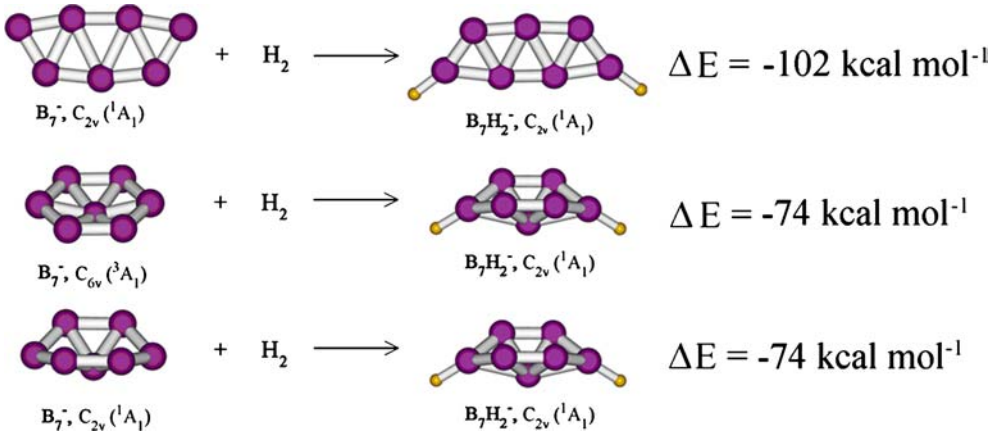

Fig. 6 Calculated hydrogenation energies (at the CCSD(T)/6-311 + G(2df) level of theory) for the lowest B_7^- isomers

HOMO-5 in $B_7H_2^-$, and HOMO, HOMO′, HOMO-1, HOMO-1′, HOMO-2, and HOMO-4 in B_7^- are responsible for the bonding over the whole system. As has been reported earlier [16], the triplet species **1** is doubly aromatic. The HOMO-4 ($1a_{2u}$) in Fig. 5b is a completely bonding π-MO and the HOMO-2 ($4a_{1g}$) is a completely bonding σ-MO. Degenerate pairs HOMO ($1e_{1g}$) and HOMO-1 ($2e_{1u}$) are partially bonding MOs of π- and σ-radial types, respectively. Thus the structure 1 is σ-aromatic (six σ-electrons) and π-aromatic (four π-electrons with single occupancy of the every degenerate HOMO). In the second isomer of B_7^- (singlet structure 2, Fig. 1), the HOMO (Fig. 5b) is doubly occupied, leaving the second degenerate MO unoccupied. Thus, the regular 4*n* Hückel's rule governs the shape of the cluster, making it π-antiaromatic. However, the second lowest isomer of $B_7H_2^-$ (structure 5, Fig. 2) possesses double antiaromaticity. The HOMO-5 ($1b_{3u}$) and HOMO ($1b_{2\,g}$) are π-MOs populated by four electrons, and thus the system is π-antiaromatic. The HOMO-2 ($4a_g$) and HOMO-1 ($3b_{2u}$) are σ-radial MOs populated by four σ-electrons, and thus the system is also σ-antiaromatic. Hence, upon hydration the most stable triplet B_7^- cluster **1** loses both π- and σ-aromatic character. The singlet isomer **2** of B_7^-, being σ-aromatic and π-antiaromatic, becomes doubly antiaromatic during the hydration process.

Energy of the hydrogenation

The effect of hydrogenation on the relative stability of the B_7^- isomers can also be illustrated by the energies of reactions of hydrogenation (at the CCSD(T)/6-311++G** level of theory) (Fig. 6). One can see that the energy of the hydrogenation is significantly higher for the isomer **3** of B_7^-.

Conclusions

Using the GEGA program, we found low-energy structures of B_7^- and $B_7H_2^-$ at the B3LYP/3-21G level of theory. The low-energy species were then re-optimized at the B3LYP/6-311++G** and CCSD(T)/6-311++G** levels of theory and the results were found to be in good agreement. CASSCF(8,8)/6-311++G** calculations showed that the Hartree–Fock configuration was dominant in the CASSCF expansion, and thus our B3LYP and CCSD(T) calculations must be reliable.

The B_7^- cluster has a wheel-type quasi-planar doubly (σ- and π-) aromatic triplet C_{6v} ($^3A_1'$) global minimum, a low-lying σ-aromatic and π-antiaromatic singlet C_{2v} ($^1A_1$) isomer with a quasi-planar shape (0.7 kcal mol^{-1} above the global minimum), and a planar doubly (σ- and π-) antiaromatic C_{2v} ($^1A_1$) isomer (7.8 kcal mol^{-1} above the global minimum). Upon hydrogenation, an inversion in stability of the species occurs. The planar $B_7H_2^-$ (C_{2v}, $^1A_1$) isomer **4**, formed by the addition of two hydrogen atoms to the doubly antiaromatic C_{2v} ($^1A_1$) B_7^- isomer **3**, becomes the global minimum structure. It is 27 kcal mol^{-1} more stable than isomer **5** of $B_7H_2^-$, originated from the quasi-planar triplet wheel isomer of B_7^-. We have shown that the reason for the inversion of stability of adducts is in the loss of the doubly aromatic character in the wheel-type global minimum isomer (C_{6v}, $^3A_1$) of B_7^- upon the H_2 addition. In contrast, the planar isomer of B_7^- (C_{2v}, $^1A_1$) gains aromatic character upon addition of two hydrogen atoms, which makes it more stable.

Acknowledgments This work was supported partially by the donors of The Petroleum Research Fund (ACS-PRF# 38242-AC6), administered by the American Chemical Society, partially by the National Science Foundation (CHE-0404937), and partially by the Summer Research Institute at the Pacific Northwest National Laboratory operated by Battelle, Richland, Washington, USA.

References

1. Hanley L, Whitten JL, Anderson SL (1988) J Phys Chem 92:5803–5812
2. Hanley L, Anderson SL (1987) J Phys Chem 91:5161–5163
3. Hanley L, Anderson SL (1988) J Chem Phys 89:2848–2860
4. Hintz PA, Ruatta SA, Anderson SL (1990) J Chem Phys 92:292–303
5. Ruatta SA, Hintz PA, Anderson SL (1991) J Chem Phys 94:2833–2847
6. Hintz PA, Sowa MB, Ruatta SA, Anderson SL (1991) J Chem Phys 94:6446–6458
7. Placa SJL, Roland PA, Wynne JJ (1992) Chem Phys Lett 190:163–168
8. Bonacic-Koutecky V, Fantucci P, Koutecky J (1991) Chem Rev 91:1035–1108
9. Kato H, Yamashita K, Morokuma K (1992) Chem Phys Lett 190:361–366
10. Ray AK, Howard IA, Kanal KM (1992) Phys Rev B 45:14247–14255
11. Boustani I (1997) Phys Rev B 55:16426–16438
12. Wang ZX, Schleyer PvR (2001) Science 292:2465–2469
13. Zhai H-J, Wang LS, Alexandrova AN, Boldyrev AI, Zakrzewski VG (2003) J Phys Chem A 107:9319–9328
14. Zhai H-J, Wang LS, Alexandrova AN, Boldyrev AI (2002) J Chem Phys 117:7917–7924
15. Alexandrova AN, Boldyrev AI, Zhai HJ, Wang LS, Sheiner E, Fowler PW (2003) J Phys Chem A 107:1359–1369
16. Alexandrova AN, Boldyrev AI, Zhai H-J, Wang LS (2004) J Phys Chem A 108:3509–3517
17. Zhai H-J, Alexandrova AN, Birch KA, Boldyrev AI, Wang LS (2003) Angew Chem Int Ed 42:6004–6008
18. Zhai H-J, Kiran B, Li J, Wang LS (2003) Nat Mater 2:827–833
19. Chandrasekhar J, Jemmis ED, Schleyer PvR (1979) Tetrahedron Lett 39:3707–3710
20. Martin-Santamaria S, Rzepa HS (2000) Chem Commun 16:1503–1504
21. Präsang C, Mlodzianowska A, Sahin Y, Hofmann M, Geiseler G, Massa W, Berndt A (2002) Angew Chem Int Ed 41:3380–3382
22. Präsang C, Hofmann M, Geiseler G, Massa W, Berndt A (2002) Angew Chem Int Ed 41:1526–1529
23. Präsang C, Mlodzianowska A, Geiseler G, Massa W, Hofmann M, Berndt A (2003) Pure Appl Chem 75:1175–1182
24. Amseis P, Mesbah W, Präsang C, Hofmann M, Geiseler G, Massa W, Berndt A (2003) Organometallics 22:1594–1596
25. Mesbah W, Präsang C, Hofmann M, Geiseler G, Massa W, Berndt A (2003) Angew Chem Int Ed 42:1717–1719

26. Lipscomb WN (1963) Boron hydrides. Benjamin, New York
27. Muetterties EL (1975) Boron hydride chemistry. Academic, New York
28. Cotton FA, Wilkinson G, Murillo CA, Bochmann M (1999) Advanced inorganic chemistry, 6th edn. Wiley, New York
29. Ricca A, Bauschlicher CW Jr (1997) J Chem Phys 106:2317–2322
30. Curtiss LA, Pople JA (1989) J Chem Phys 91:4809–4812
31. Schleyer PvR, Najafian K, Mebel A (1998) Inorg Chem 37:6765–6772
32. Goss JP, Briddon PR, Jones R, Teukam Z, Ballutaud D, Jomard F, Chevallier J, Bernard M, Deneuville A (2003) Phys Rev B 68:235209–235218
33. DiLabio GA, Matusek DR (2000) Chem Phys Lett 317:597–602
34. Wang P, Orimo S, Tanabe K, Fujii H (2003) J Alloys Comp 350:218–221
35. Boustani I (1995) Chem Phys Lett 240:135–140
36. Boustani I, Quandt A, Hernandez E, Rubio A (1999) J Chem Phys 110:3176–3185
37. Boustani I (1994) Int J Quantum Chem 52:1081–1111
38. Ricca A, Bauschlicher CW Jr (1996) Chem Phys 208:233–242
39. Kato H, Tanaka E (1991) J Comput Chem 12:1097–1107
40. Alexandrova AN, Boldyrev AI, Fu Y-J, Wang X-B, Wang L-S (2004) J Chem Phys 121:5709–5719
41. Hartke B (1993) J Phys Chem 97:9973–9976
42. Deaven DM, Ho KM (1995) Phys Rev Lett 75:288–291
43. Parr RG, Yang W (1989) Density-functional theory of atoms and molecules. Oxford University Press, Oxford
44. Becke AD (1993) J Chem Phys 98:5648–5652
45. Perdew JP, Chevary JA, Vosko SH, Jackson KA, Pederson MR, Singh DJ, Fiolhais C (1992) Phys Rev B 46:6671–6687
46. Frisch MJ, Trucks GM, Schlegel HB, Scuseria GE, Robb MA, Cheeseman JR, Montgomery JA, Vreven T, Kudin KN, Burant JC, Millam JM, Iyengar SS, Tomasi J, Barone V, Mennucci B, Cossi M, Scalmani G, Rega N, Petersson GA, Nakatsuji H, Kitao O, Nakai H, Klene M, Li X, Knox JE, Hratchian HP, Cross JB, Adamo C, Jaramillo J, Gomperts R, Stratmann RE, Yazyev O, Austin AJ, Cammi R, Pomelli C, Ochterski JW, Ayala PY, Morokuma K, Voth GA, Salvador P, Dannenberg JJ, Zakrzewski VG, Dapprich S, Daniels AD, Strain MC, Farkas O, Malick DK, Rabuck AD, Raghavachari K, Foresman JB, Ortiz JV, Cui Q, Baboul AG, Clifford S, Cioslowski J, Stefanov BB, Liu A, Liashenko A, Piskorz P, Komaromi I, Martin RL, Fox DJ, Keith T, Al-Laham MA, Peng CY, Nanayakkara A, Challacombe M, Gill PMW, Johnson BG, Chen W, Wang MW, Gonzales C, Pople JA (2003) Gaussian 03, Revision A.1. Gaussian Inc., Pittsburgh
47. Krishnan R, Binkley JS, Seeger R, Pople JA (1980) J Chem Phys 72:650–654
48. Cizek J (1969) Adv Chem Phys 14:35–89
49. Knowles PJ, Hampel C, Werner H-J (1993) J Chem Phys 99:5219–5227
50. Clark T, Chandrasekhar J, Spitznagel GW, Schleyer PvR (1983) J Comput Chem 4:294–301
51. Frisch MJ, Pople JA, Binkley JS (1984) J Chem Phys 80:3265–3269
52. Hegarty D, Robb MA (1979) Mol Phys 38:1795–1812
53. Eade RHE, Robb MA (1981) Chem Phys Lett 83:362–368
54. Schlegel HB, Robb MA (1982) Chem Phys Lett 93:43–46
55. Bernardi F, Bottini A, McDouglas JJW, Robb MA, Schlegel HB (1984) Far Symp Chem Soc 19:137–147
56. Yamamoto N, Vreven T, Robb MA, Frisch MJ, Schlegel MA (1996) Chem Phys Lett 250:373–378
57. Frisch MJ, Ragazos IN, Robb MA, Schlegel HB (1992) Chem Phys Lett 189:524–528
58. Carpenter JE, Weinhold F (1988) J Mol Struct (Theochem) 169:41–62
59. Carpenter JE (1987) PhD Thesis, University of Wisconsin, Madison
60. Foster JP, Weinhold F (1980) J Am Chem Soc 102:7211–7218
61. Reed AE, Weinhold F (1983) J Chem Phys 78:4066–4073
62. Reed AE, Curtiss LA, Weinhold F (1988) Chem Rev 88:899–926
63. Schaftenaar G (1998) MOLDEN 3.4. CAOS/CAMM Center, The Netherlands